Colloid Polym Sci 276:680–689 (1998)

ORIGINAL CONTRIBUTION

A. Ziabicki
P. Sajkiewicz

Crystallization of polymers in variable external conditions. III: Experimental determination of kinetic characteristics

Received: 13 January 1998
Accepted: 27 April 1998

A. Ziabicki (✉) · P. Sajkiewicz
Polish Academy of Sciences
Institute of Fundamental
Technological Research
21 Swietokrzyska St.
PL-00 049 Warszawa
Poland

Abstract In two recent papers [1, 2] a new model of non-isothermal crystallization kinetics has been proposed. We are discussing now the possibility of experimental determination of material characteristics appearing in the model. These include relaxation time, τ, and athermal nucleation function, B_{ath}. Two kinds of experiments are discussed: isothermal and non-isothermal, with constant cooling or heating rate. The following approach should be valid for polymers characterized by not too high crystallization rates, like polyethylene terephthalate (PET), polytrimethylene terephthalate (PTT, Corterra®), polypropylene and others. Preliminary experiments on isotactic polypropylene and polyvinylidene fluoride will illustrate possibilities of the suggested experimental procedures.

Key words Non-isothermal crystallization – transient nucleation – athermal nucleation – relaxation time

Theoretical

In the development of the model [1, 2] we have been using non-linear measure of the degree of crystallinity. Instead of volume fraction of crystallinity, commonly used in the Kolmogoroff–Avrami–Evans theory of crystallization kinetics [3–5]

$$v_{cr}/v_{tot} = x \in (0, 1) , \tag{1}$$

a non-linear measure was introduced

$$P = [-\ln(1 - x)]^{1/m} \tag{2}$$

where m is the Avrami exponent.

It is evident from the definition (2) that P, unlike x, is not limited to unity but approaches infinity when time tends to infinity, or x tends to 1

$$\lim_{\substack{t\to\infty \\ x\to 1}} P = \infty . \tag{3}$$

In steady-state isothermal conditions, crystallization rate, K, and the exponent m are constants depending on temperature, stress, molecular orientation, etc.

$$K(t) \equiv dP/dt \to K_{st}(T, p, \ldots,) = \text{const} . \tag{4}$$

Steady-state crystallization rate, K_{st}, is related to isothermal Avrami rate constant, K, and inversely proportional to crystallization half-period, $t_{1/2}$

$$K_{st} = (K_m)^{1/m} \propto 1/t_{1/2} . \tag{5}$$

Early models of non-isothermal crystallization kinetics [6–8] considered variation of K in time as a result of variation of external conditions. Crystallization rate was assumed to instantaneously follow varying external conditions. This assumption reduces time-dependent crystallization rate $K(t)$ to the quasi-static relation

$$K(t) = K_{st}[T(t), p(t), \ldots,] . \tag{6}$$

The quasi-static model has been successfully used in the conditions of slow rate of change (cooling rate, $\dot{T}$, stressing rate, $\dot{p}$, etc.).

Our new model [1, 2], intended for higher rates of change, allows for two additional effects. First, variation of crystallization is assumed to lag behind the changes of external conditions, giving rise to retardation of crystallization. This effect modifies that part of crystallization which is controlled by thermal nucleation. The model assumption is introduced in the form of a postulated relaxation equation

$$dK_{th}/dt = (K_{st} - K_{th})/\tau^* \ . \tag{7}$$

There appears an additional material characteristic, relaxation (or retardation) time τ^*, dependent on changing external conditions

$$\tau^*(t) = \tau^*[T(t), p(t), \ldots,] \ . \tag{8}$$

The relaxation assumption formulated in Eq. (7) has been inspired by the kinetics of transient nucleation processes. Since crystallization rate depends on primary nucleation and nucleation-controlled growth, it seems natural to expect that its time dependence should be similar to that of nucleation rate, $\dot{N}$. The theory of transient isothermal nucleation rate, $\dot{N}$, yields, according to Collins [9]

$$\dot{N}(t)/\dot{N}_{st}(t) = \left[1 + 2\sum_{n=1}^{\infty}(-1)^n \exp[-n^2\pi^2 t/\tau]\right], \tag{9}$$

$$d(\dot{N}/\dot{N}_{st})/dt = -(2\pi^2/\tau)\left[\sum_{n=1}^{\infty}(-1)^n n^2 \exp[-n^2\pi^2 t/\tau]\right], \tag{10}$$

where $\dot{N}_{st}$ is steady-state value, and τ-relaxation time

$$\tau = 2\pi kT/\gamma D^* \ , \tag{11}$$

where $D^* = D$ $(g = g^*)$ is "growth diffusion coefficient" taken at the critical cluster size, and γ – second derivative of the free energy of cluster formation

$$\gamma = -(d^2\Delta F/dg^2)_{g=g^*} \ . \tag{12}$$

Eq. (9) predicts monotonical increase of nucleation rate from zero at $t = 0$ to saturation at $t \to \infty$. In the range of not too short times, Eq. (10) can be approximated by a single exponential function (Fig. 1)

$$\dot{N}(t)/\dot{N}_{st}(t) \cong 1 - \exp(-\pi^2 t/\tau) = 1 - \exp(t/\tau^*) \tag{13}$$

and the rate of change approaches our model (Eq. (7)) with an effective relaxation time $\tau^* = \tau/\pi^2$

$$d(\dot{N}/\dot{N}_{st})/dt \cong (\dot{N}_{st} - \dot{N})\pi^2/\tau = (\dot{N}_{st} - \dot{N})/\tau^* \ . \tag{14}$$

Relaxational effects should appear in isothermal, as well as non-isothermal conditions.

The second, athermal effect, is proportional to the rate of change (e.g. cooling rate, $\dot{T}$). The total crystallization rate, K, includes two components, and can be presented in the form [1, 2]

$$K(t) = K_{th}(t) + K_{ath}(t) = K_{th}[1 + \dot{N}_{ath}/\dot{N}_{th}]^{1/m}$$
$$= K_{th}[1 - B_{ath}\dot{T}]^{1/m} \ . \tag{15}$$

The inverse Avrami exponent, $1/m$, appearing in Eq. (15) results from the assumption that athermal effects are included only in primary nucleation.

The generalized concept of athermal nucleation in variable external conditions has been described in the first paper of this series [1]. Athermal nucleation, $\dot{N}_{ath}$ and the corresponding athermal crystallization rate contribution, K_{ath}, refer to the concept introduced by Fisher et al. [10] and generalized by Ziabicki [11]. In contrast to common ("thermal") nucleation, "athermal" nucleation (and crystallization) rates are proportional to cooling rate, $\dot{T}$, and disappear in isothermal conditions.

The additional material functions, $\tau^*(T)$ and $B_{ath}(T)$ should be found from experiments.

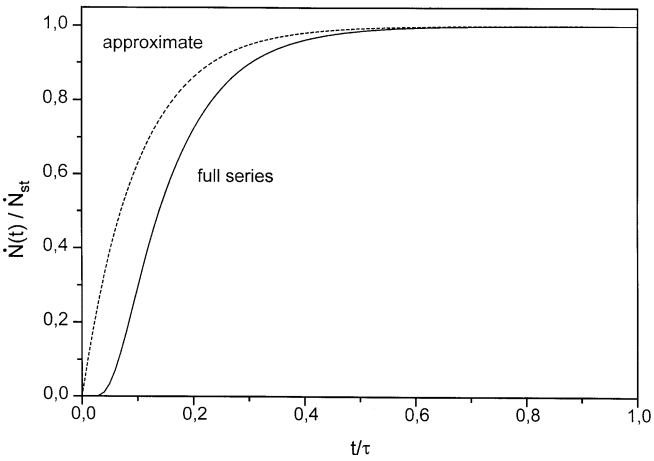

Fig. 1 Theoretical dependence of reduced nucleation rate, $\dot{N}(t)/\dot{N}_{st}$ on relative time, t/τ, "approximate" – Eq. (13), "series" – Eq. (9) with 20 terms

Transient isothermal crystallization

Determination of relaxation time, τ requires transient, isothermal measurements. The material is melted above T_m, rapidly transferred to crystallization temperature $(T < T_m)$, and the development of crystallinity is followed in time. At constant temperature, athermal effects are absent.

Originally, it was expected that relaxation time, τ^*, could be obtained from the approximate formula (13) extrapolated to zero time. Identification of $\dot{N}/\dot{N}_{st}$ with

K/K_{st} yields at the beginning of crystallization

$$\lim_{t\to 0} \mathrm{d}\ln(1 - K/K_{st})/\mathrm{d}t = -1/\tau^* \,. \tag{16}$$

Application of the approximate formula (13) at zero time is incorrect, though. In the range of short times, the behavior of $\dot{N}(t)$ (hence also $K(t)$) calculated from the full series, Eq. (9), differs from the approximate formula (13) not only quantitatively, but also qualitatively. Therefore, extrapolation of the derivative of Eq. (13) extrapolated to zero time suggested in our previous work [2] does not provide a method of determining relaxation time τ^*. As is evident from Figs. 1 and 2, the nucleation (crystallization) rate starts as a concave function of time, while the approximate model (Eq. (13)) stipulated convex relation in the entire range of times. Moreover, accuracy of experimental measurements at $t = 0$ is small and does not provide much useful information.

Figure 3 presents isothermal crystallization rate of polypropylene plotted vs. time t. The data were obtained using isothermal DSC technique. The experimental details and more data will be published separately [12]. Crystallization rate $K(t)$ starts as a concave function in agreement with the series expansion (9) presented in Figs 1 and 2. The reason for overshoot is not clear. It is possible that the shape of the plot of K vs time determined at low heat flux (early stages of crystallization) is strongly biased by limited sensitivity of the DSC instrument. It will be necessary to compare our DSC data with results obtained by other techniques.

There are two possibilities of interpreting transient isothermal crystallization experiments. First, inflexion point of crystallization rate vs time, can be used. Putting

$$\mathrm{d}^2K/\mathrm{d}t^2 = 0 \,, \tag{17}$$

Fig. 2 Theoretical dependence of reduced nucleation rate, $\dot{N}(t)/\dot{N}_{st}$ on relative time, t/τ, "approximate" – Eq. (13), "series" – Eq. (9) with 20 terms

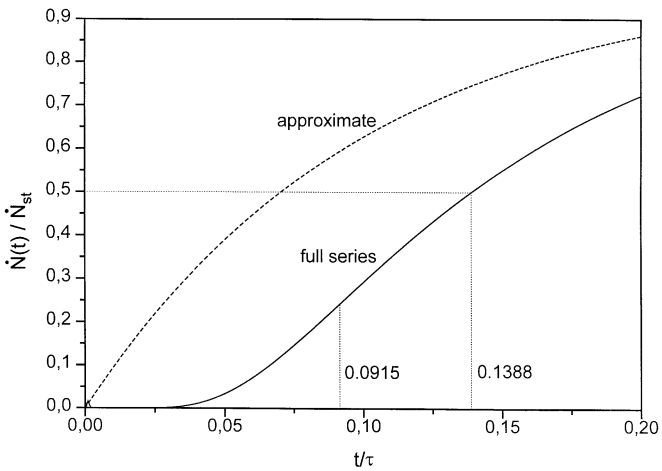

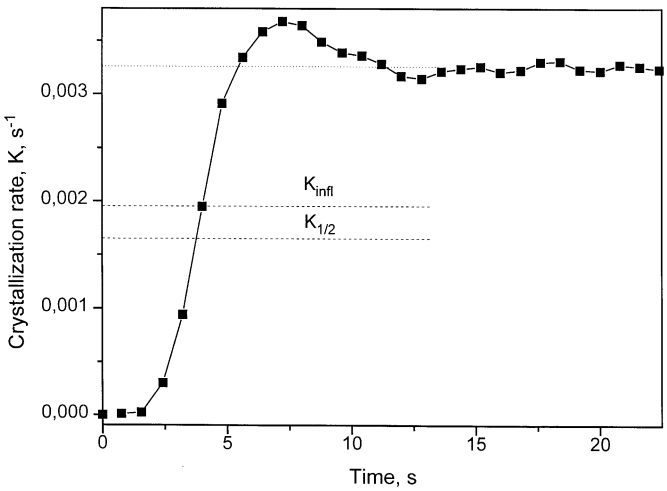

Fig. 3 Isothermal crystallization rate, K, of isotactic polypropylene at 123 °C as a function of time, t [12]

we obtain numerically from Eq. (9) (cf. Fig. 2)

$$t_{\mathrm{inf}\,l}/\tau = 0.0915 \tag{18}$$

and the effective relaxation time

$$\tau^* = \tau/\pi^2 = 1.107336\, t_{\mathrm{inf}\,l} \,. \tag{19}$$

The additional advantage of this method lies in the fact that the result does not depend on the choice of the steady-state value.

An alternative to the above procedure is finding time when nucleation rate reaches half of its maximum (saturation) value, i.e.

$$K/K_{st} = \tfrac{1}{2} \,. \tag{20}$$

From Eq. (9) it follows:

$$t_{1/2}/\tau = 0.1388 \tag{21}$$

and the effective relaxation time

$$\tau^* = \tau/\pi^2 = 0.7300\, t_{1/2} \,. \tag{22}$$

Using the data from Fig. 3, we calculated relaxation time τ^* from Eqs. (19) and (22) to obtain τ^* values listed in Table 1.

The data presented in Table 1 require further refinement and discussion. The two sets of data are reasonably consistent with each other, but two orders of magnitude shorter than "relaxation times" derived from crystallization memory experiments [13]. Limited sensitivity of the DSC instrument can lead to some underestimation of the true value of relaxation times. Further experiments using other techniques are planned.

Table 1 Relaxation times for isotactic polypropylene from Eqs. (19) and (22) [12]

Temperature, C	Effective relaxation time, τ^* (s) derived from	
	Inflexion point, Eq. (19)	Half-time, Eq. (22)
123	3.8	3.72
125	3.12	3.31
127	3.0	2.9
129	3.56	2.1

Non-isothermal crystallization at constant variation of temperature

Experiments made in non-isothermal conditions at constant cooling (or heating) rate, $\dot{T}$, provide the source of information about isothermal and non-isothermal crystallization rate characteristics. According to our model [1, 2] the total crystallization rate results in the form

$$K(t, T(t)) = \mathrm{e}^{-\xi}\left[K_0 + \int_0^{\xi(t)} \mathrm{e}^{\xi'} K_{\mathrm{st}}\,\mathrm{d}\xi'\right][1 - B_{\mathrm{ath}}\dot{T}]^{1/m}$$
$$= \mathrm{e}^{-\xi}\left[K_0 + \int_{T(0)}^{T(t)} \frac{\mathrm{e}^{\xi} K_{\mathrm{st}}(T')\,\mathrm{d}T'}{\tau^*(T')\dot{T}}\right][1 - B_{\mathrm{ath}}\dot{T}]^{1/m}$$
$$= K_{\mathrm{th}}[1 - B_{\mathrm{ath}}\dot{T}]^{1/m} . \tag{23}$$

When cooling rate is a constant different from zero, the time variable ξ

$$\xi(t) = \int_0^t \frac{\mathrm{d}t'}{\tau^*[T(t')]} , \tag{24}$$

reduces to an integral over temperature

$$\xi(t) = \xi[T(t)] = \frac{1}{\dot{T}} \int_{T(0)}^{T(t)} \frac{\mathrm{d}T'}{\tau^*(T')} . \tag{25}$$

The other material characteristic B_{ath}, is the athermal function. Thermal part of the crystallization rate, K_{th}, can be presented as a series

$$K_{\mathrm{th}}(t, T(t)) = K_0\mathrm{e}^{-\xi} + \sum_{n=0}^{\infty} (-1)^n (\partial^n K_{\mathrm{st}}/\partial\xi^n)$$
$$= K_0\mathrm{e}^{-\xi} + K_{\mathrm{st}} - (\tau^*\dot{T})(\partial K_{\mathrm{st}}/\partial T)$$
$$+ (\tau^*\dot{T})^2[\partial^2 K_{\mathrm{st}}/\partial T^2$$
$$+ \mathrm{d}\ln(\tau^*\dot{T})/\mathrm{d}T(\partial K_{\mathrm{st}}/\partial T)]$$
$$- (\tau^*\dot{T})^3[\partial^3 K_{\mathrm{st}}/\partial T^3 + \cdots] + \cdots . \tag{26}$$

The expansion variable $(\tau^*\dot{T})$ reflects physical significance of relaxational effects which disappear when either cooling rate, or relaxation time is small. At $(\tau^*\dot{T}) \to 0$, Eq. (26) returns quasi-static model of non-isothermal crystallization [6–8]

$$K_{\mathrm{th}}(t) \to K_{\mathrm{st}}[T(t)] . \tag{27}$$

We stipulate that in the initial state, crystallization rate is zero

$$K_{\mathrm{th}}(t = 0) = 0 , \tag{28}$$

which is equivalent to neglecting K_0 and initial values of the derivatives of K_{st} with respect to time

$$K_0 = \mathrm{d}K_{\mathrm{st}}/\mathrm{d}t|_{t=0} = \mathrm{d}^2K_{\mathrm{st}}/\mathrm{d}t^2|_{t=0} = \cdots = 0 . \tag{29}$$

Validity of the above assumption should be checked experimentally. The expansion (26) provides a convenient form of describing thermal crystallization rates at slow cooling. It can be presented in a compact form as

$$K_{\mathrm{th}}(t, T(t)) = K_{\mathrm{st}}(T(t))[1 + A_1\dot{T} + A_2\dot{T}^2 + A_3\dot{T}^3 + \cdots] \tag{30}$$

with

$$A_1 = -\tau^*(\partial \ln K_{\mathrm{st}}/\partial T) , \tag{30a}$$

$$A_2 = \tau^{*2}\left[\frac{1}{K_{\mathrm{st}}}(\partial^2 K_{\mathrm{st}}/\partial T^2) + (\partial \ln K_{\mathrm{st}}/\partial T)(\partial \ln \tau^*/\partial T)\right], \tag{30b}$$

$$A_3 = -\tau^{*3}\left[\frac{1}{K_{\mathrm{st}}}(\partial^3 K_{\mathrm{st}}/\partial T^3) + \frac{3}{K_{\mathrm{st}}}(\partial^2 K_{\mathrm{st}}/\partial T^2)(\partial \ln \tau^*/\partial T)\right.$$
$$\left. + (\partial \ln K_{\mathrm{st}}/\partial T)[(\partial^2 \ln \tau^*/\partial T^2) + 2(\partial \ln \tau^*/\partial T)^2]\right] . \tag{30c}$$

The athermal correction (second factor in Eq. (23) can also be expanded in series to yield

$$[1 - B_{\mathrm{ath}}\dot{T}]^{1/m} = 1 + B_1\dot{T} + B_2\dot{T}^2 + B_3\dot{T}^3 + \cdots \tag{31}$$

with

$$B_1 = -B_{\mathrm{ath}}/m , \tag{31a}$$

$$B_2 = (1 - m)B_{\mathrm{ath}}^2/m^2 , \tag{31b}$$

$$B_3 = (1 - m)(1 - 2m)B_{\mathrm{ath}}^3/m^3 . \tag{31c}$$

Consequently, expansion of the total (non-isothermal) crystallization rate assumes the form

$$K(t, T(t)) = K_{\mathrm{th}}(t, T(t))[1 - B_{\mathrm{ath}}\dot{T}]^{1/m}$$
$$= K_{\mathrm{st}}[1 + (A_1 + B_1)\dot{T} + (A_2 + B_2 + A_1B_1)\dot{T}^2$$
$$+ (\cdots)\dot{T}^3 + \cdots] . \tag{32}$$

Integration of the crystallization rate over time

$$P(t) \equiv [-\ln(1-x(t))]^{1/m} \equiv \int_0^t K(t')\,\mathrm{d}t' \tag{33}$$

can be replaced by integration over temperature, when cooling rate, $\dot{T}$, is a constant different from zero

$$\begin{aligned} P(t) \to P[T(t)] &= \frac{1}{\dot{T}} \int_{T(0)}^{T(t)} K(T')\,\mathrm{d}T' \\ &= \frac{1}{\dot{T}} \int_{T(0)}^{T(t)} K_{\mathrm{st}}(T')\{1 + (A_1(T') \\ &\quad + B_1(T')]\,\dot{T} + [A_2(T') + B_2(T') \\ &\quad + A_1(T')B_1(T')]\,\dot{T}^2 + \cdots\}\,\mathrm{d}T' \,. \end{aligned} \tag{34}$$

This procedure is possible only in nonisothermal conditions. Note that there is no continuous transition at $\dot{T} = 0$ between Eq. (34) and the isothermal integral Eq. (4).

Performing non-isothermal crystallization runs at different (constant) cooling (heating) rates yields information required for analysis of the material functions τ^* and B_{ath}. Evaluation of experimental data is based on the comparison of crystallinities, $P(\dot{T}; T)$, found at the same final temperature, T, and different (constant) cooling/heating rates, $\dot{T}$.

For polymers, steady-state crystallization rate exhibits a maximum at $T = T_{\max}$, and drops to zero in the vicinity of melting temperature, T_{m}, and near glass transition temperature, T_{g}. This is schematically shown in Fig. 4. Depending on the temperature range, different experimental situations can be analyzed.

High-temperature crystallization. Cooling from the melt

When the starting temperature, $T(0)$, lies well above the upper crystallization temperature (melting temperature) T_{m}, the conditions (28–29) are satisfied, and the rate of temperature change, $\dot{T}$, is negative (cooling). We will analyze the plot of the product $(-\dot{T}\cdot P)$ vs absolute cooling rate, $(-\dot{T})$. The intercept

$$\lim_{\dot{T}\to 0} (-\dot{T}\cdot P) = \int_{T(t)}^{T(0)} K_{\mathrm{st}}(T')\,\mathrm{d}T' \tag{35}$$

yields a positive material function, integral of the steady-state crystallization rate taken from a given temperature, T, to the upper crystallization limit $T(0)$. The choice of $T(0)$ is unimportant as far as it is located beyond the crystallization range (above T_{m}). Differentiation of the intercept with respect to end temperature yields steady-state crystallization rate $K_{\mathrm{st}}(T)$

$$K_{\mathrm{st}}(T) = -\frac{\mathrm{d}}{\mathrm{d}T} \lim_{\dot{T}\to 0} (-\dot{T}\cdot P) \,. \tag{36}$$

Sometimes, non-isothermal procedure may yield steady-state crystallization rates in the low-temperature region inaccessible to standard isothermal experiments. An example will be shown in Fig. 9.

The initial slope

$$\lim_{\dot{T}\to 0} \mathrm{d}(-\dot{T}\cdot P)/\mathrm{d}(-\dot{T}) = -\int_{T(t)}^{T(0)} K_{\mathrm{st}}(T')(A_1(T') + B_1(T'))\,\mathrm{d}T' \tag{37}$$

is controlled by the sum of relaxation and athermal effects

$$A_1 + B_1 = -\tau^*(\partial \ln K_{\mathrm{st}}/\partial T) - B_{\mathrm{ath}}/m \,. \tag{38}$$

The first term, related to relaxation effects in the upper branch of the crystallization curve, is positive, the second one (athermal) – negative. When athermal effects dominate over relaxation ($|B_1| > |A_1|$), the observed product $|\dot{T}\cdot P|$ will increase with cooling rate, $|\dot{T}|$; when $|B_1| < |A_1|$ – the reverse is true. The sum of relaxational and athermal coefficients is obtained from differentiation of the initial slope and division by previously determined steady-state crystallization rate

$$A_1(T) + B_1(T) = \frac{1}{K_{\mathrm{st}}(T)} \frac{\mathrm{d}}{\mathrm{d}t} \left[\lim_{\dot{T}\to 0} \frac{\mathrm{d}(-\dot{T}\cdot P)}{\mathrm{d}(-\dot{T})} \right]. \tag{39}$$

Analysis of the second derivative at $\dot{T} = 0$ yields initial curvature of the crystallization curve.

$$\lim_{\dot{T}\to 0} \frac{\mathrm{d}^2(-\dot{T}\cdot P)}{\mathrm{d}(-\dot{T})^2} = 2\int_{T(t)}^{T(0)} K_{\mathrm{st}}(A_2 + B_2 + A_1B_1)\,\mathrm{d}T' \,. \tag{40}$$

Consider sign of the sum

$$\begin{aligned} A_2 + B_2 + A_1B_1 &= \tau^{*2}\left[\frac{1}{K_{\mathrm{st}}}(\partial^2 K_{\mathrm{st}}/\partial T^2) + (\partial \ln K_{\mathrm{st}}/\partial T)(\partial \ln \tau^*/\partial T)\right] \\ &\quad + (1-m)B_{\mathrm{ath}}^2/m^2 + \tau^*(\partial \ln K_{\mathrm{st}}/\partial T)B_{\mathrm{ath}}/m \,. \end{aligned} \tag{41}$$

When crystallization is dominated by athermal effects, the most important terms, $B_2 = (1-m)B_{\mathrm{ath}}^2/m^2$, and A_1B_1 are negative, and the $(-\dot{T}\cdot P)$ curve starts as an increasing convex function of the cooling rate. When relaxation dominates over athermal nucleation, the curvature depends on temperature. Curvature of the steady-state crystallization rate, and the related part of the A_2 coefficient (proportional to $\partial^2 K_{\mathrm{st}}/\partial T^2$, cf. Fig. 4) is negative in the range of temperatures between $T_{\max}$ and $T_{\mathrm{infl},2}$ (upper inflexion point) and positive above $T_{\mathrm{infl},2}$. The A_1B_1 terms are

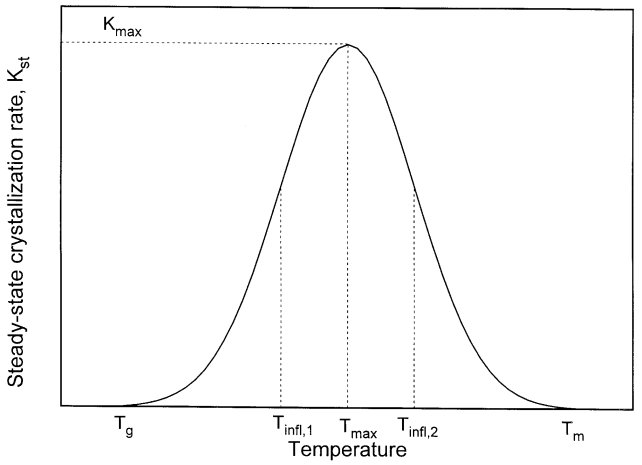

Fig. 4 Steady-state crystallization rate, K_{st}, as a function of temperature, T (schematic). Maximum crystallization rate, T_{max}, and two inflexion points ($T_{infl,1}$, $T_{infl,1}$) indicated. T_g – glass transition temperature, T_m – melting temperature

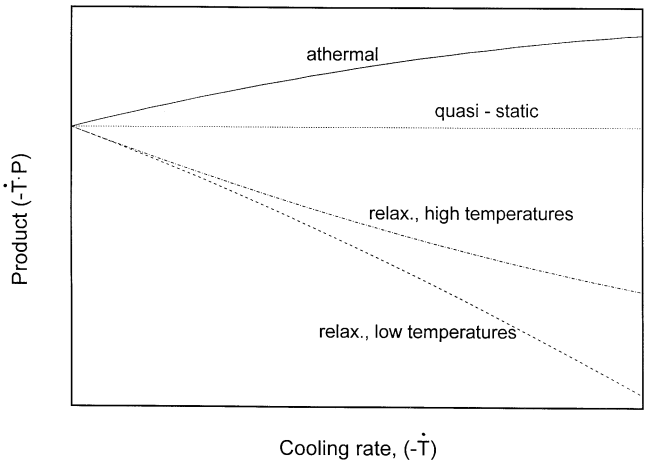

Fig. 5 Expected shapes of the $(-\dot{T}\cdot P)$ vs. $(-\dot{T})$ plot in constant cooling rate experiments

always negative. Therefore, curvature of the product $(-\dot{T}\cdot P)$ plotted vs cooling rate, $(-\dot{T})$ changes sign, being positive at higher crystallization temperatures (concave behavior), and negative (convex) at smaller temperatures, close to T_{max}. Various shapes of the $(-\dot{T}\cdot P)$ vs $(-\dot{T})$ curves are shown schematically in Fig. 5.

Experimental

Figure 6 presents the experimental data for polyvinylidene fluoride Kynar 880 N (Pennwalt Co.) with $M_w = 400\,000$. The data were obtained using Perkin-Elmer DSC-7 apparatus calibrated with indium during heating at 10°/min. Additional correction for the temperature lag between the sample and the furnace according to the method proposed by Janeschitz–Kriegl et al. [14] was performed. The samples were crystallized at constant cooling rates after being held in the molten state at 220°C for 10 min. As seen in Fig. 6 the initial slope is positive, and curvature negative, suggesting determining role of athermal effects.

Figures 7 and 8 present, respectively, the intercept (Eq. (35)) and initial slope (Eq. (37)) as functions of end temperature, T. Considering nonlinearity of the $(-\dot{T}\cdot P)$ vs $(-\dot{T})$ curves evident in Fig. 6, the intercept and initial slope were extrapolated from the data in the range of cooling rates between 2 and 15°/min using third order polynomial.

Differentiation of the intercept with respect to temperature (Eq. (36)) yields steady-state crystallization rate (Fig. 9).

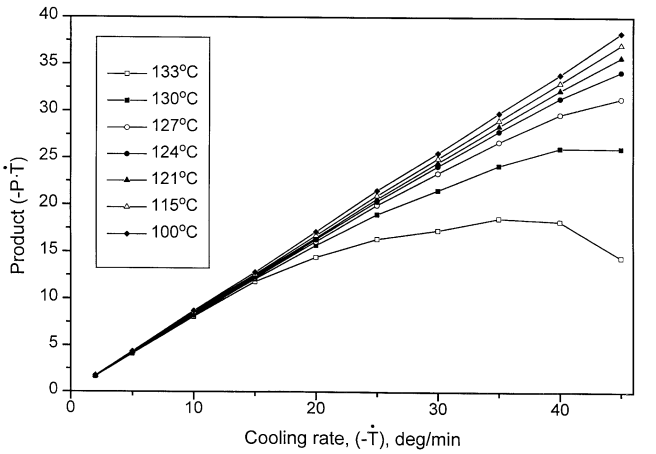

Fig. 6 Experimental $(-\dot{T}\cdot P)$ vs. $(-\dot{T})$ plot for polyvinylidene fluoride [12]. End temperatures, T, indicated

It should be noted that earlier kinetic data from isothermal crystallization of PVDF [15] did not reach the low-temperature region covered by our non-isothermal procedure. We found good agreement between the temperature of the maximum rate of steady-state crystallization of investigated PVDF and that predicted by Okui on the basis of the empirical relationship between temperature of the maximum crystallization rate and equilibrium melting temperature. Okui [16] found the ratio of T_{max}/T_m^o for several polymers being in the range between 0.76 and 0.89. Putting $T_m^o = 481.3$ K as equilibrium melting temperature of the α phase with 0% content of head-to-head defect [17] and $T_{max} = 388.2$ K as a temperature of maximum

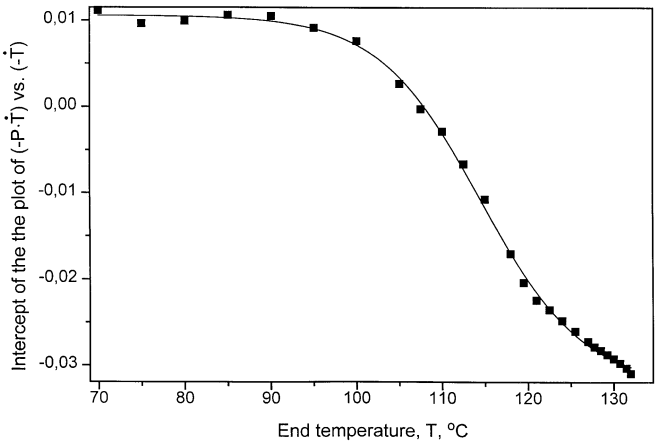

Fig. 7 Intercept of the $(-\dot{T}\cdot P)$ vs. $(-\dot{T})$ plot for polyvinylidene fluoride vs end temperature T [12]

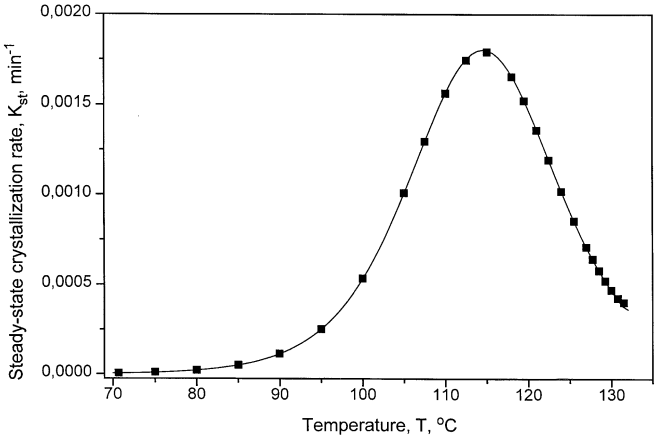

Fig. 9 Steady-state crystallization rate K_{st} for polyvinylidene fluoride derived from the intercept of Fig. 6 via Eq. (36)

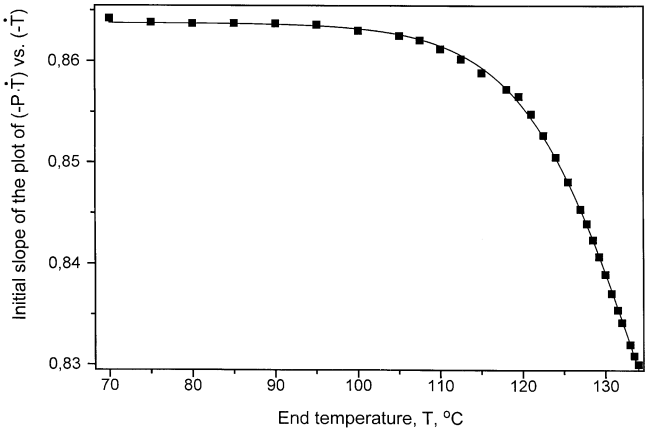

Fig. 8 Initial slope of the $(-\dot{T}\cdot P)$ vs. $(-\dot{T})$ plot for polyvinylidene fluoride vs end temperature, T [12]

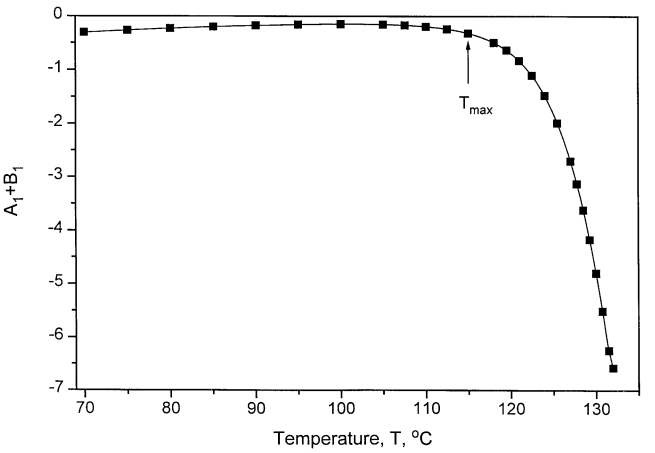

Fig. 10 The sum of relaxational and athermal effects $(A_1 + B_1)$ for polyvinylidene fluoride derived from the initial slope in Fig. 6 via Eq. (39)

steady-state crystallization rate determined from our data we get the ratio of $T_{max}/T_m^o = 0.806$.

The sum of relaxational and athermal effects obtained from Eq. (39) is plotted vs temperature in Fig. 10. In the whole range of crystallization temperatures the sum $(A_1 + B_1)$ is negative which indicates domination of athermal nucleation. It is seen in the upper branch of crystallization curve that athermal effects increase with temperature.

Low-temperature crystallization. Heating from the glassy state

In another experimental setup, polymer melt is rapidly quenched below the glass transition. Crystallization in the frozen amorphous material starts below glass transition temperature $(T(0) < T_g)$ and is induced by heating in the lower branch of the crystallization rate. Crystallization temperatures usually are kept below T_{max}.

In the conditions of heating, both the relaxation (A_1) and athermal coefficients (B_1) are negative, and the product $(\dot{T}\cdot P)$ should decrease with increasing heating rate, $\dot{T}$ (Fig. 11). When crystallization is dominated by athermal effects, the B_2 term is negative and the initial behavior of the product $(\dot{T}\cdot P)$ is convex. The behavior controlled by relaxational effects admits positive and negative curvature, as a result of the change of the coefficient A_2: the low-temperature part of A_2 (between T_g and the left inflexion point $T_{infl,1}$) is concave, the upper one (between $T_{infl,1}$ and

T_{max})-convex. These predictions are shown schematically in Fig. 11.

Global non-isothermal effects

For evaluation of the global intensity of non-isothermal effects, crystallization with constant cooling rate should be performed over the entire range of crystallization temperatures, starting above melting temperature, ending below glass transition. The corresponding crystallinities, $P_\infty(\dot{T})$ are functions of cooling rate only, and the observed product $(-\dot{T}\cdot P)$ results in the form

$$-\dot{T}P_\infty(\dot{T}) = -\int_{T_g}^{T_m} K_{st}\,dT + \dot{T}\int_{T_g}^{T_m} K_{st}(A_1 + B_1)\,dT + \cdots . \tag{42}$$

The first integral representing quasi-static crystallization is a positive, material constant characterizing "crystallizability" of the polymer [6]. The kernel of the second integral may change sign and general discussion of its contribution is difficult. The initial slope and shape of the experimental $(-\dot{T}\cdot P)$ vs $(-\dot{T})$ curve yield rough information about the sensitivity of crystallization to cooling rate, and about the appropriate combinations of the integral material characteristics $A_{i,\infty}$, $B_{i,\infty}$, defined as

$$A_{i,\infty} = \int_{T_g}^{T_m} K_{st}(T)\cdot A_i(T)\,dT , \tag{43}$$

$$B_{i,\infty} = \int_{T_g}^{T_m} K_{st}(T)\cdot B_i(T)\,dT . \tag{44}$$

The above procedure requires non-zero cooling rate, and does not reduce to Avrami equation when $\dot{T} = 0$.

Fig. 11 Expected shapes of the $(\dot{T}\cdot P)$ vs. $(\dot{T})$ plot in constant heating rate experiments

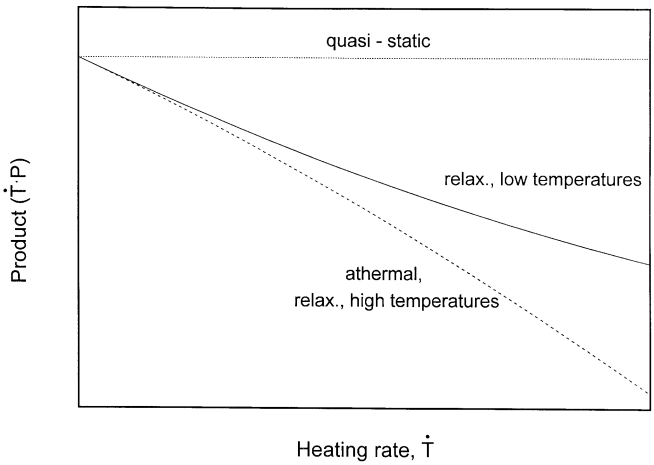

Athermal effects revisited

In the previous paper [2] we have tried to evaluate athermal contribution to non-isothermal crystallization rate for polypropylene (PP) and polyethylene terephthalate (PET). The analysis was based on the theory of nucleation and, rather arbitrarily assumed, relaxation times, τ^*. The uncertainty concerned relaxation times as such, and the relation between τ^* and the "diffusion of growth coefficient", D^*. Our earlier calculations suggested much stronger effects for PP (with very long relaxation times estimated from memory effects, Ref. [13] than for PET. For both polymers, however, athermal contribution was negligible, except for temperatures close to T_m.

We will reconsider this problem to provide information about the relative significance of athermal and relaxational effects in the expansion coefficients A_i, B_i (Eqs. (30) and (31)). We consider the third polymer – polyvinylidene fluoride – which has been subject to preliminary experimental studies [12]. We will show that both, A_i and B_i, include relaxation time in the power i. Consequently, the magnitude of relaxation time does not affect the balance between various mechanisms which control non-isothermal crystallization kinetics.

The ratio of athermal-to-thermal nucleation rate in Eq. (31) results in the form [2]

$$-B_{ath}\dot{T} \equiv \dot{N}_{ath}/\dot{N}_{th} = \dot{T}(\partial g^*/\partial T)\rho(g^*)/D^*(\partial\rho/\partial g)_{|g=g^*} \cong -\tfrac{3}{2}\dot{T}(\partial g^*/\partial T)g^*/D^* . \tag{45}$$

The relation between the "diffusion of growth" coefficient, D^* and relaxation time, τ, will now be taken after Collins [9] as in Eqs. (11) and (12). Taking into account that second gradient of cluster formation free energy is

$$\gamma \equiv -(d^2\Delta F/dg^2)_{g=g^*} = \tfrac{4}{3}\sigma v_0^{2/3}(g^*)^{-4/3} , \tag{46}$$

$$\frac{\partial g^*}{\partial T} = \frac{3g^*}{\Delta T} , \tag{47}$$

we arrive at the ratio

$$\dot{N}_{ath}/\dot{N}_{th} = -3(\dot{T}\tau)(g^*)^{2/3}\sigma v_0^{2/3}/\pi kT\Delta T = -3\pi(\dot{T}\tau^*)(g^*)^{2/3}\sigma v_0^{2/3}/kT\,\Delta T , \tag{48}$$

where $\tau^* = \tau/\pi^2$ denotes effective relaxation time [9]. Taking into account that

$$g^* = \frac{64\sigma^3 T_m^3}{\Delta h^3 \Delta T_0^3 v_0} , \tag{49}$$

where σ is interface tension, Δh the heat of melting per unit volume, v_0 the molecular volume of a single kinetic unit (segment), ΔT the undercooling, we obtain

$$\dot{N}_{ath}/\dot{N}_{th} = -48\pi(\dot{T}\tau^*)\sigma^3 T_m^2/kT\,\Delta T^3\,\Delta h^2 . \tag{50}$$

Table 2 Nucleation and crystallization characteristics for isotactic polypropylene, polyethylene terephthalate and polyvinylidene fluoride

Data	*i*-PP	Ref.	PET	Ref.	PVDF	Ref.
Heat of fusion, Δh, 10^9 [erg/cm]	1.4	[19]	1.8	[20]	2.01	[23]
Ave. interface tension, σ, [erg]/cm	23	[19]	27	[20]	18.3	[23]
Melting temperature, T_m [K]	481.2	[19]	553	[21]	493	[23]
Max. cryst. temperature, T_{max} [K]	338.2	[18, 22]	463.2	[18, 21]		
Half-width of the cryst. rate-temperature curve, D [deg]	30	[18, 22]	32	[18, 21]		

Consequently, the first athermal expansion coefficient

$$B_1 \equiv B_{ath}/m = (\dot{N}_{ath}/\dot{N}_{th})/m\dot{T}$$
$$= -48(\pi/m)\tau^*\sigma^3 T_m^2/kT\,\Delta T^3\,\Delta h^2 \quad (51)$$

appears to be proportional to relaxation time, τ^*. Similarly, higher athermal coefficients, B_i, are proportional to the corresponding powers of τ^*

$$B_i = (B_1)^i(1-m)(1-2m)\cdots(1-i\cdot m+m) \propto (\tau^*)^i\,, \quad (52)$$

which converts expansion of the total crystallization rate, Eq. (32) into a unique expansion over the variable $(\dot{T}\tau^*)$

$$K(\dot{T}, T) = K_{st}(T)[1 + (A_1' + B_1')(\dot{T}\tau^*)$$
$$+ (A_2' + B_2' + A_1'B_1')(\dot{T}\tau^*)^2 + \cdots] \quad (53)$$

$A_i' = A_i/(\tau^*)^i$ and $B_i' = B_i/(\tau^*)^i$ are expansion coefficients reduced by the appropriate powers of the relaxation time, τ^*.

Domination of either athermal or relaxational effects in non-isothermal crystallization does not depend on the magnitude of τ^*.

We will compare absolute values of the reduced coefficients A_1' and B_1' for three polymers: PP, PET and PVDF. B_1' will be calculated from Eq. (51) with $m = 3$, yielding

$$B_1' = 16\pi\sigma^3 T_m^2/kT\,\Delta T^3\,\Delta h^2 \quad (54)$$

and A_1' from Eq. (30a) with Gaussian crystallization rate function

$$K_{st}(T) = K_{max}\exp[-4\ln 2(T - T_{max})^2/D^2]\,, \quad (55)$$

yielding

$$A_1' = -\partial \ln K_{st}/\partial T = 8\ln 2(T - T_{max})/D^2\,. \quad (56)$$

The material functions used in the calculations (the same as in Ref [2]) are given in Table 2.

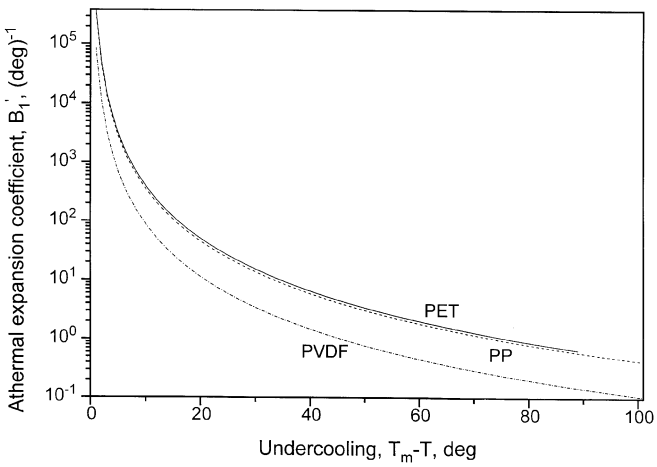

Fig. 12 Reduced athermal coefficients, B_1' for isostatic polypropylene (PP), polyethylene terephthalate (PET) and polyvinylidene fluoride (PVDF) calculated from Eq. (54) as a function of undercooling, ΔT. Material characteristics from Table 2

Our considerations can be applied to other polymers with not too high crystallization rates, like poly-trimethylene terephthalate (PTT, Corterra®), syndiotactic polystyrene, etc. What is needed for such an extension is material characteristics (thermodynamic and kinetic) like those listed in Table 2.

Figure 12 presents athermal coefficients, B_1' calculated from Eq. (54) for isotactic polypropylene (PP), polyethylene terephthalate (PET) and polyvinylidene fluoride (PVDF).

It is evident that, in contrast to our earlier estimates [2], the behavior of PP and PET is practically identical; the data for PVDF show the same trend, but are smaller, apparently due to smaller surface tension, σ, and higher heat of fusion, Δh. Comparison of thermal and athermal coefficients (A_1' from Eq. (56), B_1' from Eq. (54) suggests (Fig. 13) that within the range of 100° below melting

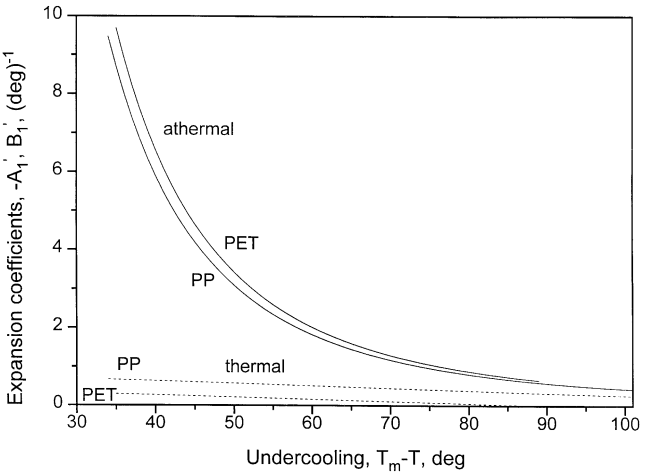

Fig. 13 Reduced thermal (dotted lines, A'_1) and athermal expansion coefficients, (solid lines, B'_1) for isotactic polypropylene (PP) and polyethylene terephthalate (PET) calculated from Eqs. (56) and (54) as functions of undercooling, ΔT. Material characteristics from Table 2

temperature, the dominating mechanism is athermal nucleation.

Discussion

It has been shown how material characteristics of the recently developed model of non-isothermal crystallization [1, 2] can be derived from isothermal and non-isothermal kinetic studies. Preliminary experiments on polypropylene and polyvinylidene fluoride using differential scanning calorimetry (DSC) seem to yield reasonable and reproducible results. Strong acceleration of crystallization by fast cooling can be explained by athermal nucleation. Experimental testing comparing isothermal and non-isothermal crystallization will be continued using DSC and other techniques.

Acknowledgement The authors acknowledge partial support offered by Shell Chemical Co., Houston TX.

References

1. Ziabicki A (1996) Colloid Polym Sci 274:209
2. Ziabicki A (1996) Colloid Polym Sci 274:705
3. Kolmogoroff AN (1937) Izvestiya Akad Nauk SSSR, Ser Math 3:335
4. Avrami M (1939) J Chem Phys 7:1103
5. Evans UR (1945) Trans Faraday Soc 41:365
6. Ziabicki A (1967) Appl Polymer Symposia 6:1
7. Nakamura K, Watanabe T, Katayama K, Amano T (1972) J Appl Polymer Sci 16:1077 ibid (1973) 17:1031
8. Ozawa T (1971) Polymer 12:150
9. Collins FC (1955) Zf Elektrochem 59:404
10. Fisher JC, Hollomon JH, Turnbull D (1948) J Appl Phys 19:775
11. Ziabicki A (1986) J Chem Phys 85:3042
12. Sajkiewicz P, to be published
13. Alfonso GC, Ziabicki A (1995) Colloid Polym Sci 273:317
14. Janeschitz-Kriegl H, Wippel H, Paulik Ch, Eder G (1993) Colloid Polym Sci 271:1107
15. Mancarella C, Martuscelli E (1977) Polymer 18:1240
16. Okui N (1987) Polymer J 19:1309
17. Chen LT, Frank CW (1984) Ferroelectrics 57:51
18. Ziabicki A (1976) Fundamentals of Fibre Formation. Wiley, London
19. Monasse B, Haudin JM (1986) Colloid Polym Sci 264:117
20. Palys LH, Phillips PJ (1980) J Polym Sci (Phys) 18:829
21. Cobbs WH, Burton RL (1953) J Polym Sci 50:275
22. Magill JH (1962) Polymer 3:35
23. Marand HL, Stein RS, Stack GM (1989) J Polym Sci (Phys) 27:1089